


Article

Degradation of Ketamine and Methamphetamine by the UV/H₂O₂ System: Kinetics, Mechanisms and Comparison

De-Ming Gu ^{1,2}, Chang-Sheng Guo ¹ , Qi-Yan Feng ², Heng Zhang ¹ and Jian Xu ^{1,*}

¹ Center for Environmental Health Risk Assessment and Research, Chinese Research Academy of Environmental Sciences, Beijing 100012, China; goodmingaust@163.com (D.-M.G.); guocs@craes.org.cn (C.-S.G.); zhangheng_craes@163.com (H.Z.)

² School of Environment Science and Spatial Informatics, China University of Mining and Technology, Xuzhou 221116, China; fqycumt@126.com

* Correspondence: xujian@craes.org.cn

Received: 31 August 2020; Accepted: 22 October 2020; Published: 26 October 2020



Abstract: The illegal use and low biodegradability of psychoactive substances has led to their introduction to the natural water environment, causing potential harm to ecosystems and human health. This paper compared the reaction kinetics and degradation mechanisms of ketamine (KET) and methamphetamine (METH) by UV/H₂O₂. Results indicated that the degradation of KET and METH using UV or H₂O₂ alone was negligible. UV/H₂O₂ had a strong synergizing effect, which could effectively remove 99% of KET and METH (100 µg/L) within 120 and 60 min, respectively. Their degradation was fully consistent with pseudo-first-order reaction kinetics ($R^2 > 0.99$). Based on competition kinetics, the rate constants of the hydroxyl radical with KET and METH were calculated to be 4.43×10^9 and $7.91 \times 10^9 \text{ M}^{-1}\cdot\text{s}^{-1}$, respectively. The apparent rate constants of KET and METH increased respectively from 0.001 to 0.027 and 0.049 min^{-1} with the initial H₂O₂ dosage ranging from 0 to 1000 µM at pH 7. Their degradation was significantly inhibited by HCO₃⁻, Cl⁻, NO₃⁻ and humic acid, with Cl⁻ having relatively little effect on the degradation of KET. Ultraperformance liquid chromatography with tandem mass spectrometry was used to identify the reaction intermediates, based on which the possible degradation pathways were proposed. These promising results clearly demonstrated the potential of the UV/H₂O₂ process for the effective removal of KET and METH from contaminated wastewater.

Keywords: ketamine; methamphetamine; UV/H₂O₂; degradation kinetics; reaction intermediates

1. Introduction

Illicit drugs are nonprescribed or psychostimulant substances which cannot be completely removed by conventional wastewater treatment, resulting in their widespread occurrence in aquatic environments [1,2]. Ketamine (KET) and methamphetamine (METH) were detected most frequently, with concentration levels up to 275 ng/L for KET and 239 ng/L for METH, in surface waters in China [3]. METH removal at most wastewater treatment plants was more than 80%, while the elimination of KET was less than 50% or even negative [4]. It was confirmed that chronic environmental concentrations of METH can lead to health issues in aquatic organisms [5]. Liao et al. [6] also reported that blood circulation and incubation time in medaka fish embryos could be significantly delayed at environmental concentration levels (0.004–40 µM) of KET and METH, which altered the swimming behavior of medaka fish larvae. Thus, there is an urgent need to explore new, efficient methods for eliminating these emerging contaminants in water.

Advanced oxidation processes (AOPs) have been employed to destroy illicit drugs due to their high efficiency and lower environmental impact [7,8]. The UV/H₂O₂ process is one of the AOPs and generates the strong, oxidizing hydroxyl radical ($\bullet\text{OH}$, $E_0 = 2.72\text{ V}$), which attacks the organic compounds with rate constants ranging from 10^8 to $10^{10}\text{ M}^{-1}\text{ s}^{-1}$ [9]. Benzoylcegonine (BE), a metabolite of cocaine, was effectively removed by UV/H₂O₂ from different matrices [10]. The degradation of KET and METH was investigated using various AOPs, but no available report, so far, has addressed $\bullet\text{OH}$ assisted by UV/H₂O₂ treatment. After 3 min, 100 $\mu\text{g/L}$ of METH that had been added to deionized water was completely eliminated by TiO₂ photocatalysis under UV_{365nm} irradiation [11]. Wei et al. [12] studied the synthesis of a novel sonocatalyst Er³⁺:YAlO₃/Nb₂O₅ and its application for METH degradation. Gu et al. [13] observed that complete removal of KET was achieved by UV/persulfate, and possible transformation pathways were proposed.

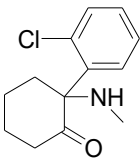
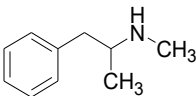
To the best of our knowledge, there is little information about the theoretical calculation of the reactivity of KET and METH by radical attack using the UV/H₂O₂ process. Water constituents in actual wastewater could affect the degradation efficacy; therefore, a comprehensive understanding of the degradation of KET and METH using the UV/H₂O₂ system is needed. The aim of this study was to investigate the degradation kinetics and mechanisms of KET and METH during the UV/H₂O₂ process. The influence of various parameters on KET and METH removal was evaluated, including initial H₂O₂ dosage, pH and water background components. The degradation products were analyzed by ultraperformance liquid chromatography with tandem mass spectrometry (UPLC-MS/MS), and possible transformation paths were proposed.

2. Materials and Methods

2.1. Materials

The KET and METH were obtained from Cerilliant Corporation (Round Rock, TX); detailed information is listed in Table 1. HPLC grade acetonitrile (ACN) and methanol (MeOH) were purchased from Fisher Scientific (Poole, UK). Formic acid (FA, $\geq 98\%$) and benzoic acid (BA) were purchased from Sigma-Aldrich (Bellefonte, USA). Analytical grade H₂O₂ (30%, v/v), NaHCO₃ ($\geq 99.7\%$), NaCl ($\geq 99.0\%$), NaNO₃ ($\geq 99.5\%$), NaOH ($\geq 99.5\%$), humic acid (HA) and H₂SO₄ ($\geq 98\%$) were obtained from Sinopharm Chemical Reagent Co., Ltd. (Beijing, China). All reaction solutions were configured with Milli-Q water produced by an ultrapure water system (Millipore, MA, USA).

Table 1. Chemical structures and properties of ketamine and methamphetamine.

Compound	Chemical Formula	Structure	CAS Number	pKa	Log K _{ow}
Ketamine	C ₁₃ H ₁₆ ClNO		6740-88-1	7.5	2.18
Methamphetamine	C ₁₀ H ₁₅ N		4846-07-5	9.9	2.07

2.2. Experimental Section

The experiments were operated in the quartz tubes (25 mm in diameter and 175 mm in length), which were placed in a photochemical reactor (Figure 1, XPA-7, Xujiang Machinery Factory, Nanjing, China). A low-pressure mercury lamp (11 W, emission at 254 nm, Philips Co., Zhuhai, China) was placed in the quartz sleeve. The UV lamp was preheated for 30 min to ensure irradiation stability. The UV fluence rate of 0.1 mW cm^{-2} was determined using three different methods [14]. The newly configured KET/METH and H₂O₂ stock solutions were supplemented with appropriate volumes to achieve a

50 mL reaction solution, which was then stirred thoroughly at 300 rpm with electromagnetic stirrers. Upon UV irradiation, the reaction started at pH 7.0 and room temperature. Specific samples were immediately quenched using a catalase and passed through 0.22 μm nylon filter before further analysis.

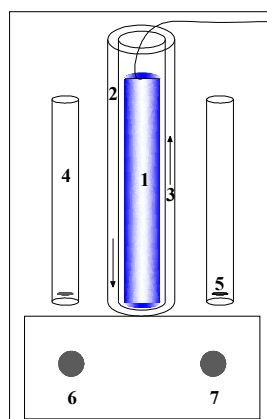


Figure 1. The schematic diagram of the experiment setup: (1) low-pressure Hg UV lamp, (2) quartz tube, (3) cooling water, (4) photoreactor, (5) magnetic stirrer, (6) magnetic stirrer apparatus, (7) thermostat.

2.3. Analytical Methods

The concentrations of KET and METH were quantified by UPLC-MS/MS equipped with a Waters Acquity liquid chromatography system and an Xevo T_{QS} triple quadrupole mass spectrometer (Waters Co., Milford, MA, USA). The analytes were separated by a reverse phase column (Acquity UPLC BEH C18, 1.7 μm , 50 \times 2.1 mm, Waters, MA, USA). The mobile phases A and B, with a flow rate of 450 $\mu\text{L min}^{-1}$, were 0.1% FA in Milli-Q water and ACN, respectively. Ten percent of phase B was kept for 0.5 min at the initial proportion, linearly increased to 45% at 1.8 min, then increased to 95% within 0.1 min, held for 1.0 min, reverted to 10% at 3.0 min and held for 1.5 min. The injection volume was 5 μL with the column temperature at 40 $^{\circ}\text{C}$. The chromatograms were recorded in the positive ion multiple reaction monitoring (MRM) mode. Nitrogen was used as the desolvation and nebulizing gas. The capillary voltage was set at 0.5 kV, and the desolvation temperature was 400 $^{\circ}\text{C}$. Optimized UPLC-MS/MS parameters are given in Table 2.

Table 2. Detailed ultraperformance liquid chromatography with tandem mass spectrometry (UPLC-MS/MS) parameters for ketamine and methamphetamine.

Compound	Parent Ion (m/z)	Retention Time (min)	Production (m/z)	Cone Voltage (V)	Collision Voltage (V)
Ketamine	238	1.31	125	16	24
			179	16	16
Methamphetamine	150	1.11	91	22	16
			119	22	10

3. Results and Discussion

3.1. Degradation Kinetics of KET and METH

Figure 2 shows the degradation of KET and METH under different treatment processes. UV or H_2O_2 alone exhibited negligible effects on their degradation, suggesting that treatment by UV or H_2O_2 alone was unable to destroy KET and METH. However, nearly complete removal of KET and METH was achieved within 120 and 60 min, respectively, when treated with the combination of UV/ H_2O_2 . Similar results were reported regarding ofloxacin degradation, which was drastically increased due to the large amount of hydroxyl radicals ($\bullet\text{OH}$) generated via the breakage of the H_2O_2

bond (Equation (1)) [15]. The degradation of KET and METH was consistent with the pseudo-first-order reaction kinetics. The apparent degradation rate constants (k_{obs}) of KET and METH by UV/H₂O₂ were 0.027 and 0.049 min⁻¹, respectively.

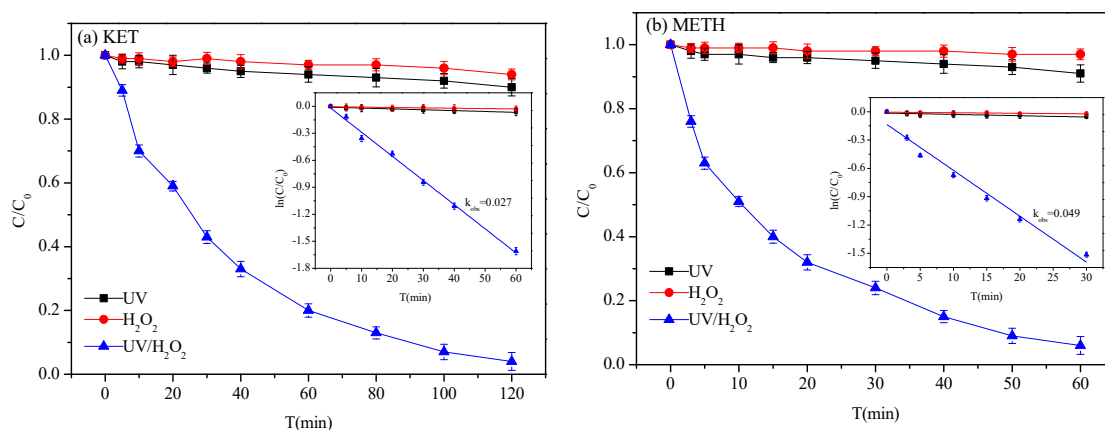


Figure 2. Degradation kinetics of ketamine (KET) (a) and methamphetamine (METH) (b) by different treatments. Conditions: Initial concentrations of KET and METH = 100 µg/L, Initial concentration of hydrogen peroxide (H₂O₂)₀ = 500 µM, pH₀ = 7.0, Temperature (T) = 25 ± 1 °C.

3.2. Determination of Bimolecular Reaction Rate

The generation of $\bullet\text{OH}$ in the UV/H₂O₂ system was proved by the photoluminescence (PL) technique using a probe molecule with terephthalic acid, which tends to react with $\bullet\text{OH}$ to form 2-hydroxyterephthalic acid, a highly fluorescent product [16]. The PL intensity of 2-hydroxyterephthalic acid is proportional to the amount of $\bullet\text{OH}$ radicals produced in water [17]. Figure 3 shows the PL spectral changes in the 5×10^{-4} M terephthalic acid solution with a concentration of 2×10^{-3} M NaOH (excitation at 315 nm), as described by Yu et al. [17]. Similar fluorescence intensity was found in the reaction systems with initial concentrations of 100 and 1000 µM of H₂O₂, suggesting a constant concentration of $\bullet\text{OH}$ with the initial H₂O₂ dosage ranging from 100 to 1000 µM. The PL signal at 425 nm increased with the irradiation time, which was attributed to the reaction of terephthalic acid with $\bullet\text{OH}$ generated in the UV/H₂O₂ system.

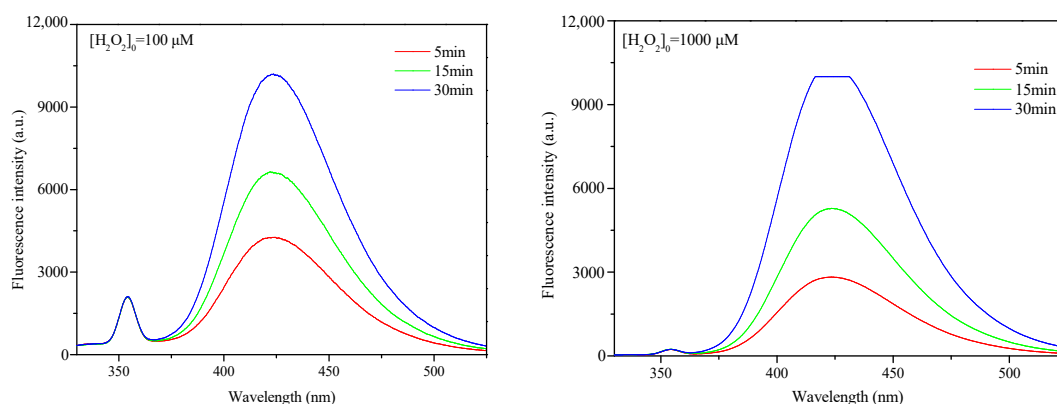


Figure 3. Photoluminescence (PL) spectral changes observed in the UV/H₂O₂ system in a 5×10^{-4} M basic solution of terephthalic acid (excitation at 315 nm).

The bimolecular reaction rates of KET and METH reacting with $\bullet\text{OH}$ were determined through the competition experiments at pH 7 (phosphate buffer solution, 5 mM). BA was used as the reference compound, with which the constant reaction rate of $\bullet\text{OH}$ is known to be $5.9 \times 10^9 \text{ M}^{-1} \text{ s}^{-1}$ [18]. It is important to note that the degradation of KET, METH and BA using UV alone was negligible at less than 9%. Equations (2) and (3) describe the competing kinetics of KET and METH with $\bullet\text{OH}$ in the UV/ H_2O_2 oxidation process, through which the bimolecular reaction rates of KET and METH reacting with $\bullet\text{OH}$ were 4.43×10^9 and $7.91 \times 10^9 \text{ M}^{-1} \text{ s}^{-1}$, respectively (Figure 4).

$$\ln \frac{(\text{KET})_0}{(\text{KET})_t} = \frac{k_{\bullet\text{OH-KET}}}{k_{\bullet\text{OH-BA}}} \ln \frac{(\text{BA})_0}{(\text{BA})_t} \quad (2)$$

$$\ln \frac{(\text{METH})_0}{(\text{METH})_t} = \frac{k_{\bullet\text{OH-METH}}}{k_{\bullet\text{OH-BA}}} \ln \frac{(\text{BA})_0}{(\text{BA})_t} \quad (3)$$

where $(\text{KET})_0$, $(\text{METH})_0$ and $(\text{BA})_0$ are the initial concentrations ($\mu\text{mol/L}$) of target compounds. $(\text{KET})_t$, $(\text{METH})_t$ and $(\text{BA})_t$ are the concentrations ($\mu\text{mol/L}$) at time t (min). $k_{\bullet\text{OH-KET}}$, $k_{\bullet\text{OH-METH}}$ and $k_{\bullet\text{OH-BA}}$ are the bimolecular reaction rates of KET, METH and BA reacting with $\bullet\text{OH}$, respectively.

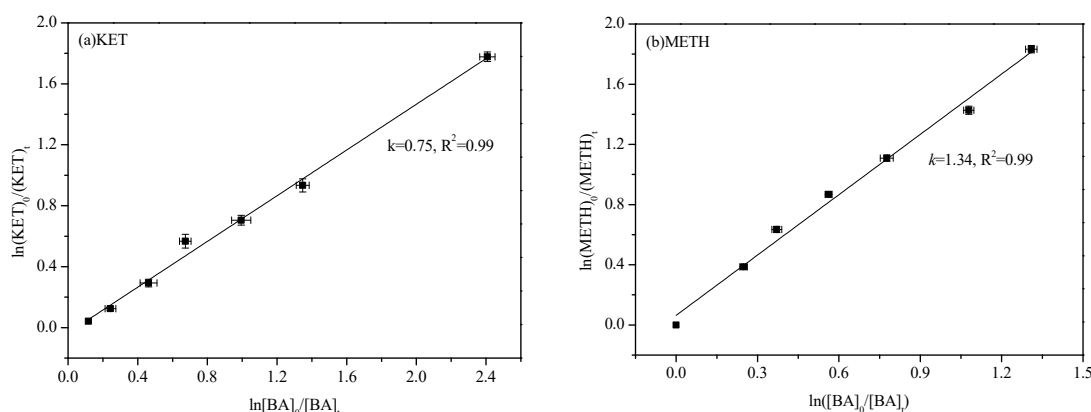


Figure 4. (a) The reaction rate constant of KET with $\bullet\text{OH}$. Conditions: $(\text{KET})_0 = (\text{BA})_0 = 0.42 \mu\text{M}$, $(\text{H}_2\text{O}_2)_0 = 1 \text{ mM}$, pH = 7, $T = 25 \pm 1 \text{ }^\circ\text{C}$. (b) The reaction rate constant of METH with $\bullet\text{OH}$. Conditions: $(\text{METH})_0 = (\text{BA})_0 = 0.67 \mu\text{M}$, $(\text{H}_2\text{O}_2)_0 = 1 \text{ mM}$, pH = 7, temperature = $25 \pm 1 \text{ }^\circ\text{C}$.

3.3. Effect of H_2O_2 Dosage

The KET and METH degradation under different initial H_2O_2 dosages were consistent with the pseudo-first-order reaction model ($R^2 > 0.99$, Figure 5). The k_{obs} of KET and METH increased dramatically from 0.001 min^{-1} to 0.027 and 0.049 min^{-1} with the initial H_2O_2 dosage ranging from 0 to $1000 \mu\text{M}$. The reason for this phenomenon is that the production of $\bullet\text{OH}$ increased with the initial H_2O_2 dosage ranging from 0 to $1000 \mu\text{M}$, thus accelerating the degradation rate of target compounds [19]. However, the k_{obs} of METH decreased slightly with the initial concentration of H_2O_2 increased to $2000 \mu\text{M}$. A similar phenomenon was observed in a previous report that indicated that the degradation rates of cyclophosphamide and 5-fluorouracil were proportional to the H_2O_2 dosage and slightly decreased with excess H_2O_2 [20]. An excessive amount of H_2O_2 would cause the self-scavenging effect of $\bullet\text{OH}$ to form $\text{HO}_2\bullet$ and $\text{O}_2^-\bullet$ (Equations (4) and (5)) [21], the low reactivity of which could reduce the degradation rate. Similar results were obtained concerning the degradation of ofloxacin [15] and chloramphenicol [22]. Moreover, large amounts of $\bullet\text{OH}$ were dimerized to H_2O_2 , and the generated $\text{HO}_2\bullet$ and $\text{O}_2^-\bullet$ subsequently participated in other reactions (Equations (6)–(9)) [23]. This negative effect was not observed in this study, probably because the maximum H_2O_2 dosage ($2000 \mu\text{M}$) was not high enough to inhibit the KET degradation.



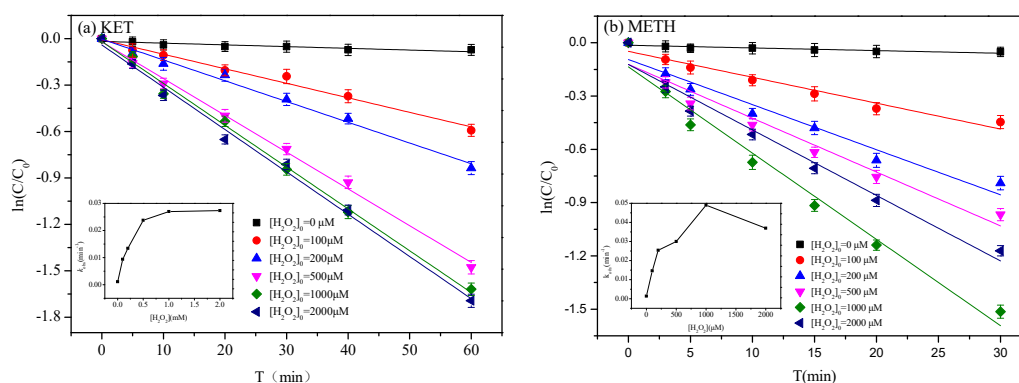
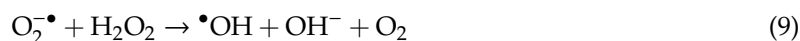
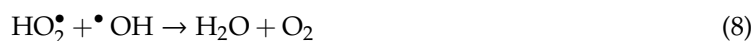
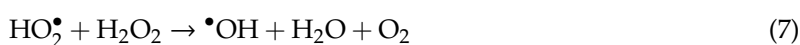
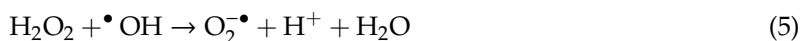


Figure 5. Effect of H_2O_2 dosage on KET (a) and METH (b) degradation in the UV/ H_2O_2 system. Conditions: $(\text{KET})_0 = (\text{METH})_0 = 100 \mu\text{g/L}$, $(\text{H}_2\text{O}_2)_0 = 0\text{--}2000 \mu\text{M}$, $\text{pH}_0 = 7.0$, $T = 25 \pm 1 \text{ }^\circ\text{C}$.

3.4. Effect of Initial pH

Figure 6 illustrates the KET and METH destruction at different initial pHs, which were adjusted with an H_2SO_4 or NaOH solution (0.1 M). No buffer was used due to its inhibiting effect on the decomposition of organics [24]. The KET and METH degradation at different initial pHs followed the pseudo-first-order reaction model well. The k_{obs} of KET and METH reached the highest levels in a neutral environment at 0.027 and 0.085 min^{-1} , respectively. Due to the greater stability of H_2O_2 at pH 5 and 7, the degradation rates of KET and METH under acidic and neutral conditions were obviously better than those under alkaline conditions. Under alkaline conditions, $\bullet\text{OH}$ could be quenched by the HO_2^- produced by H_2O_2 dissociation, thus reducing the yield of $\bullet\text{OH}$ in the system.

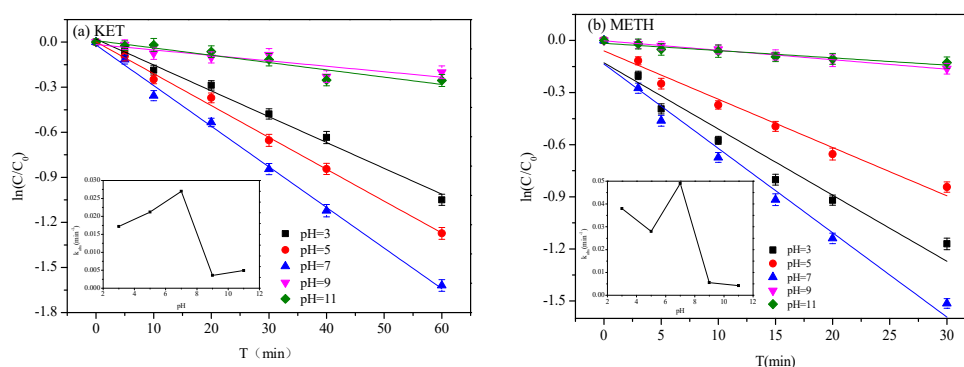


Figure 6. Effects of different initial pHs on the degradation of KET (a) and METH (b) in the UV/ H_2O_2 system. Conditions: $(\text{KET})_0 = (\text{METH})_0 = 100 \mu\text{g/L}$, $(\text{H}_2\text{O}_2)_0 = 500 \mu\text{M}$, $\text{pH}_0 = 3\text{--}11$, $T = 25 \pm 1 \text{ }^\circ\text{C}$.

3.5. Effect of Water Background Components on Degradation Efficiency of Target Compounds

There are many different substrates in natural water, including different kinds of anions, cations and organic matter. These ions could react with free radicals in advanced oxidation processes, thus inhibiting or promoting the reaction and affecting the overall oxidation effect. Therefore, it is of

great significance to study the influence of different ion types and contents on the practical application of advanced oxidation technology.

3.5.1. Effect of HCO_3^-

The decomposition of KET and METH was significantly inhibited with the addition of HCO_3^- at different initial dosages in the UV/ H_2O_2 oxidation process (Figure 7). When the initial dosage of HCO_3^- ranged from 0 to 10 mM, the reaction rate of KET and METH decreased from 0.027 and 0.049 min^{-1} to 0.008 and 0.011 min^{-1} , respectively. The reason for this experimental phenomenon was that HCO_3^- was the quenching agent for $\bullet\text{OH}$ which was also consumed by the competing reaction of ionized CO_3^{2-} (Equations (10)–(13)). Therefore, the inhibitory effect of KET and METH degradation was more obvious with the increase of the HCO_3^- concentration.

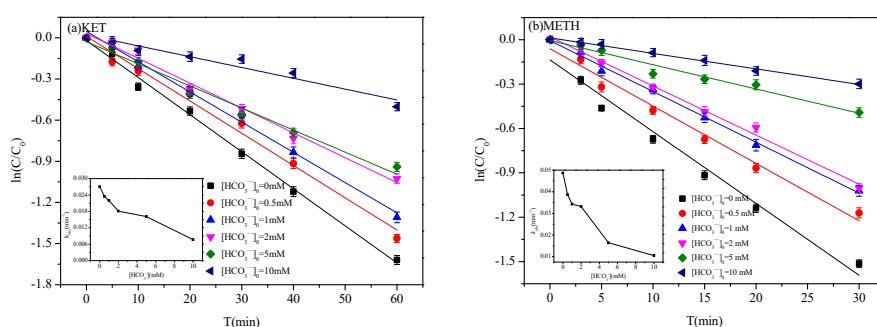
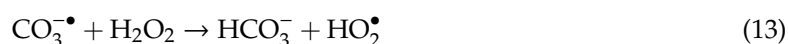
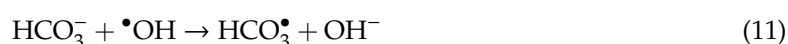


Figure 7. Effect of HCO_3^- on KET (a) and METH (b) degradation in UV/ H_2O_2 system. Conditions: $(\text{KET})_0 = (\text{METH})_0 = 100 \mu\text{g/L}$, $(\text{H}_2\text{O}_2)_0 = 500 \mu\text{M}$, $\text{pH}_0 = 7.0$, $T = 25 \pm 1 \text{ }^\circ\text{C}$.

3.5.2. Effect of Cl^-

With the initial concentration of Cl^- ranging from 0 to 10 mM, the destruction of KET was dramatically inhibited with the rate constant of KET decreased from 0.027 to 0.018 min^{-1} (Figure 8), which could be due to the elimination of $\bullet\text{OH}$ by Cl^- according to Equations (14)–(16) [25]. The degradation reaction rate changed slightly as more Cl^- was added. However, the METH degradation was less affected by Cl^- , with the reaction rate remaining basically unchanged (0.0446–0.0485 min^{-1}).

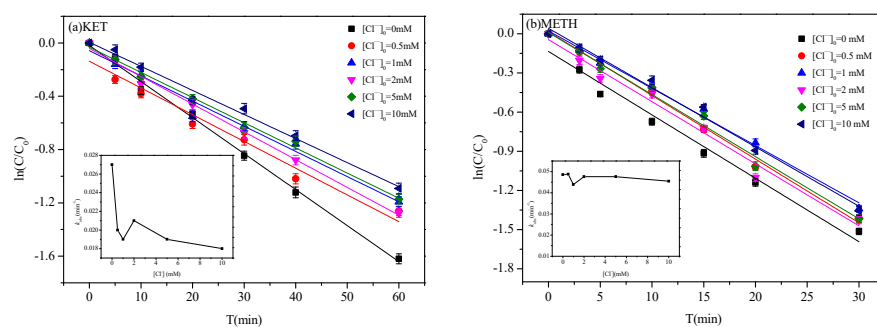


Figure 8. Effect of Cl^- on KET (a) and METH (b) degradation in the UV/ H_2O_2 system. Conditions: $(\text{KET})_0 = (\text{METH})_0 = 100 \mu\text{g/L}$, $(\text{H}_2\text{O}_2)_0 = 500 \mu\text{M}$, $\text{pH}_0 = 7.0$, $T = 25 \pm 1 \text{ }^\circ\text{C}$.

3.5.3. Effect of NO_3^- 

The influence of NO_3^- on the decomposition of KET and METH is illustrated in Figure 9. With the initial concentration of NO_3^- ranging from 0 to 10 mM, the degradation of both target compounds was obviously inhibited. The reaction rate of KET and METH decreased from 0.027 and 0.049 min^{-1} to 0.007 and 0.012 min^{-1} , respectively. The above experimental phenomena were attributed to the following: First, a large amount of $\bullet\text{OH}$ could be produced from NO_3^- under UV irradiation (Equations (17)–(18)), which is an important source of $\bullet\text{OH}$ in natural water [26]. Second, as a photosensitizer, NO_3^- has a strong absorption in the ultraviolet range, which results in the formation of an internal filter that prevents the effective light transmittance and leads to the decline of $\bullet\text{OH}$ production in the UV/ H_2O_2 system [27]. The latter was found to be dominant after the degradation effect of the reaction was analyzed.

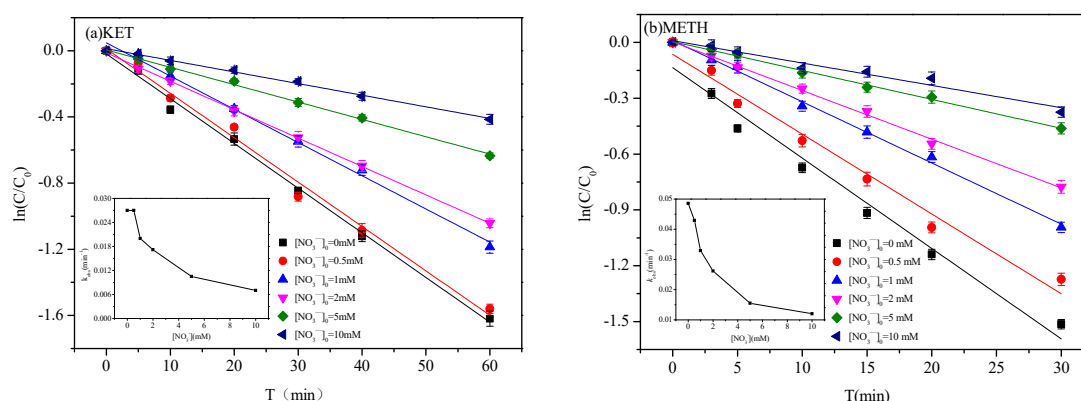


Figure 9. Effect of NO_3^- on KET (a) and METH (b) degradation in the UV/ H_2O_2 system. Conditions: $(\text{KET})_0 = (\text{METH})_0 = 100 \mu\text{g/L}$, $(\text{H}_2\text{O}_2)_0 = 500 \mu\text{M}$, $\text{pH}_0 = 7.0$, $T = 25 \pm 1 \text{ }^\circ\text{C}$.

3.5.4. Effect of HA

Due to its complex structure, HA may have uncontrollable effects on the destruction of target compounds. As illustrated in Figure 10, KET and METH degradation was dramatically inhibited once HA was added with different dosages in the UV/ H_2O_2 system. As more HA (0–0.1 mM) was added, the reaction rate of KET and METH declined from 0.027 and 0.049 min^{-1} to 0.001 and 0.008 min^{-1} , respectively, while the degradation reaction rate changed slightly with the continued addition of the HA. UV irradiation was absorbed by HA, creating an inner filter (Figure 11) and significantly inhibiting the UV transmittance for UV photons, thus limiting the generation of $\bullet\text{OH}$ in the UV/ H_2O_2 process [28]. Moreover, the degradation of target compounds can be inhibited by the competing reaction of HA with the active radicals [29].

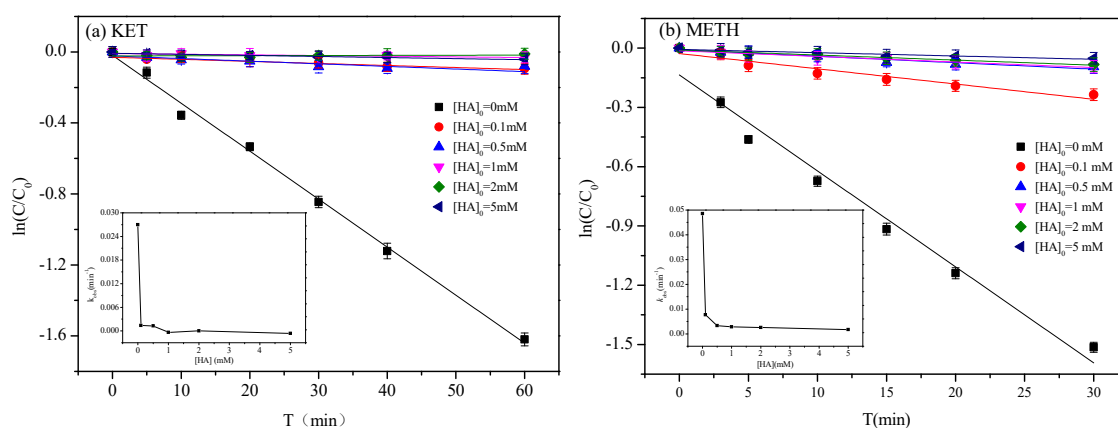


Figure 10. Effect of HA on KET (a) and METH (b) degradation in the UV/H₂O₂ system. Conditions: (KET)₀ = (METH)₀ = 100 µg/L, (H₂O₂)₀ = 500 µM, pH₀ = 7.0, T = 25 ± 1 °C.

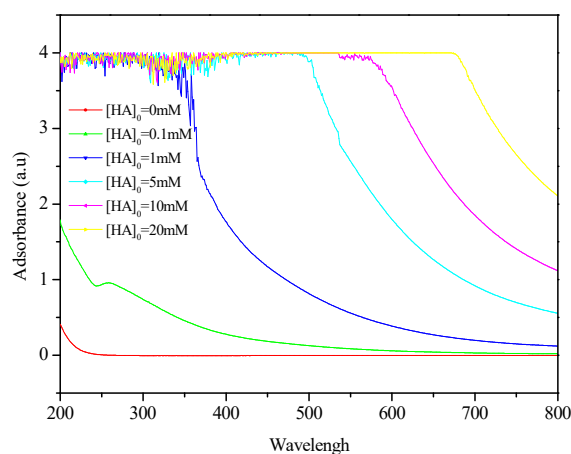


Figure 11. The ultraviolet–visible spectroscopy of reaction solutions at different concentrations of HA.

3.6. Degradation Products and Mechanism

Degradation intermediates and products of METH produced in the UV/H₂O₂ oxidation process were determined by using UPLC/MS/MS under full scans and product ion scans. During the whole METH degradation process, the mass spectra were compared to identify the intermediates. The structure of the transformation products was analyzed with the specific molecular ions and fragmentation patterns rather than direct comparison with corresponding standards. Figure 12 illustrates the mass spectra and possible structures of the degradation intermediates, based on which the possible transformation pathways of METH during UV/H₂O₂ are shown in Figure 13. The proposed degradation mechanisms of METH degradation involved in the UV/H₂O₂ system include hydrogenation, hydroxylation and electrophilic substitution.

With the molecular weight of 149, intermediate product 2 (P2, $m/z = 150$) was formed as a result of hydrogenation of METH. P1 ($m/z = 91$) with a stable structure was generated from the fracture of the C-C bond of the branched chain. Intermediates P3 ($m/z = 110$) and P4 ($m/z = 73$) were formed by electrophilic substitution of hydroxyl. METH was hydroxylated to form ephedrine ($m/z = 165$), of which the C-C bond of branched chain was fractured to form intermediate product P5 ($m/z = 57$). The hydroxylation of ephedrine induced the formation of intermediate P6 ($m/z = 181$) which was then achieved to form intermediate P7 ($m/z = 89$) after further hydroxylation. The mineralization of KET and METH was characterized by removal of total organic carbon (TOC), which achieved 41% and 57% within 60 min under UV/H₂O₂ treatment (Figure 14). The intermediate products were further degraded as the reaction continued.

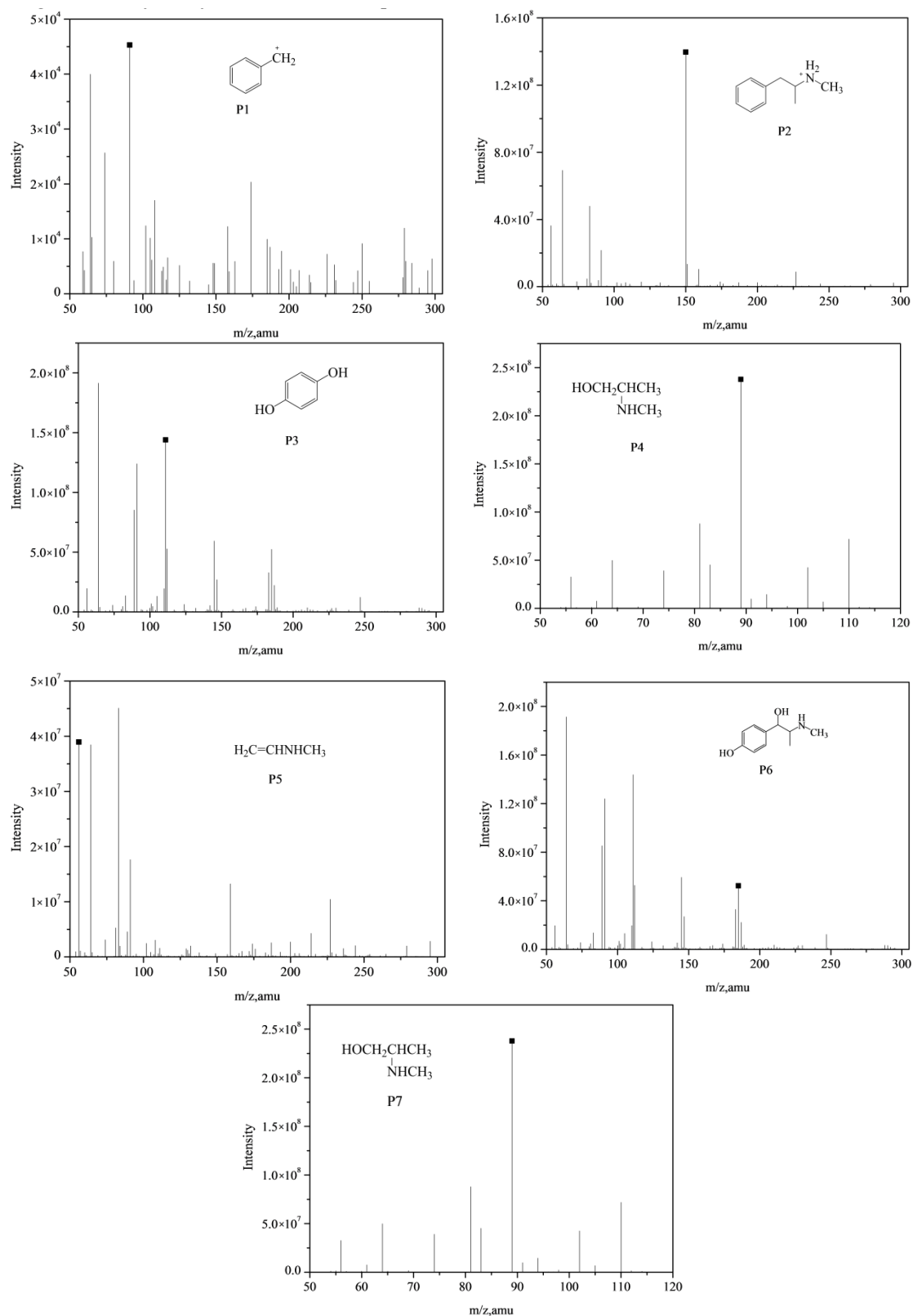


Figure 12. Mass spectra of the intermediate products of METH in the UV/PS system.

Funding: This work was funded by the National Natural Science Foundation of China (NSFC, 41673120) and Beijing Natural Science Foundation (8173058).

Acknowledgments: This study was carried out as part of the NSFC project, managed by the Jian Xu and supported by Center for Environmental Health Risk Assessment and Research, Chinese Research Academy of Environmental Sciences. We thank Wenli Qiu for her help in operating HPLC-MS. Reviewers are also thanked for the time dedicated and their comments.

Conflicts of Interest: The authors declare no conflict of interest.

References

1. Baker, D.R.; Kasprzyk-Hordern, B. Spatial and temporal occurrence of pharmaceuticals and illicit drugs in the aqueous environment and during wastewater treatment: New developments. *Sci. Total Environ.* **2013**, *454–455*, 442–456. [[CrossRef](#)]
2. Bijlsma, L.; Serrano, R.; Ferrer, C.; Tormos, I.; Hernández, F. Occurrence and behavior of illicit drugs and metabolites in sewage water from the Spanish Mediterranean coast (Valencia region). *Sci. Total Environ.* **2014**, *487*, 703–709. [[CrossRef](#)] [[PubMed](#)]
3. Wang, Z.; Xu, Z.; Li, X. Biodegradation of methamphetamine and ketamine in aquatic ecosystem and associated shift in bacterial community. *J. Hazard. Mater.* **2018**, *359*, 356–364. [[CrossRef](#)] [[PubMed](#)]
4. Du, P.; Li, K.; Li, J.; Xu, Z.; Fu, X.; Yang, J.; Zhang, H.; Li, X. Methamphetamine and ketamine use in major Chinese cities, a nationwide reconnaissance through sewage-based epidemiology. *Water Res.* **2015**, *84*, 76–84. [[CrossRef](#)] [[PubMed](#)]
5. Santos, M.E.S.; Grabicová, K.; Steinbach, C.; Schmidt-Posthaus, H.; Randák, T. Environmental concentration of methamphetamine induces pathological changes in brown trout (*Salmo trutta fario*). *Chemosphere* **2020**, *254*, 126882. [[CrossRef](#)] [[PubMed](#)]
6. Liao, P.H.; Hwang, C.C.; Chen, T.H.; Chen, P.J. Developmental exposures to waterborne abused drugs alter physiological function and larval locomotion in early life stages of medaka fish. *Aquat. Toxicol.* **2015**, *165*, 84–92. [[CrossRef](#)] [[PubMed](#)]
7. Awual, M.R.; Hasan, M.M. A ligand based innovative composite material for selective lead(II) capturing from wastewater. *J. Mol. Liq.* **2019**, *294*, 111679. [[CrossRef](#)]
8. Awual Rabiul, M. A novel facial composite adsorbent for enhanced copper(II) detection and removal from wastewater. *Chem. Eng. J.* **2015**, *266*, 368–375. [[CrossRef](#)]
9. Neta, P.; Huie, R.E.; Ross, A.B. Rate Constants for Reactions of Inorganic Radicals in Aqueous Solution. *J. Phys. Chem. Ref. Data* **1988**, *17*, 1027–1284. [[CrossRef](#)]
10. Russo, D.; Spasiano, D.; Vaccaro, M.; Cochran, K.H.; Richardson, S.D.; Andreozzi, R.; Puma, G.L.; Reis, N.M.; Marotta, R. Investigation on the removal of the major cocaine metabolite (benzoylecgonine) in water matrices by UV₂₅₄/H₂O₂ process by using a flow microcapillary film array photoreactor as an efficient experimental tool. *Water Res.* **2015**, *89*, 375–383. [[CrossRef](#)]
11. Kuo, C.; Lin, C.; Hong, P.A.K. Photocatalytic degradation of methamphetamine by UV/TiO₂—Kinetics, intermediates, and products. *Water Res.* **2015**, *74*, 1–9. [[CrossRef](#)] [[PubMed](#)]
12. Wei, C.; Yi, K.; Sun, G.; Wang, J. Synthesis of novel sonocatalyst Er³⁺:YAlO₃/Nb₂O₅ and its application for sonocatalytic degradation of methamphetamine hydrochloride. *Ultrason. Sonochem.* **2018**, *42*, 57–67. [[CrossRef](#)]
13. Gu, D.; Guo, C.; Hou, S.; Lv, J.; Zhang, Y.; Feng, Q.; Zhang, Y.; Xu, J. Kinetic and mechanistic investigation on the decomposition of ketamine by UV-254 nm activated persulfate. *Chem. Eng. J.* **2019**, *370*, 19–26. [[CrossRef](#)]
14. He, X.; Pelaez, M.; Westrick, J.A.; O’Shea, K.E.; Hiskia, A.; Triantis, T.; Kaloudis, T.; Stefan, M.I.; Armah, A.; Dionysiou, D.D. Efficient removal of microcystin-LR by UV-C/H₂O₂ in synthetic and natural water samples. *Water Res.* **2012**, *46*, 1501–1510. [[CrossRef](#)] [[PubMed](#)]
15. Lin, C.C.; Lin, H.Y.; Hsu, L.J. Degradation of ofloxacin using UV/H₂O₂ process in a large photoreactor. *Sep. Purif. Technol.* **2016**, *168*, 57–61. [[CrossRef](#)]
16. Cheng, B.; Le, Y.; Yu, J. Preparation and enhanced photocatalytic activity of Ag@TiO₂ core-shell nanocomposite nanowires. *J. Hazard. Mater.* **2010**, *177*, 971–977. [[CrossRef](#)]
17. Yu, X.; Liu, S.; Yu, J. Superparamagnetic γ -Fe₂O₃@SiO₂@TiO₂ composite microspheres with superior photocatalytic properties. *Appl. Catal. B Environ.* **2011**, *104*, 12–20. [[CrossRef](#)]

18. Ismail, L.; Ferronato, C.; Fine, L.; Jaber, F.; Chovelon, J.M. Elimination of sulfaclozine from water with SO_4^- radicals: Evaluation of different persulfate activation methods. *Appl. Catal. B Environ.* **2016**, *201*, 573–581. [[CrossRef](#)]
19. Znad, H.; Abbas, K.; Hena, S.; Awual, M.R. Synthesis a novel multilamellar mesoporous $\text{TiO}_2/\text{ZSM-5}$ for photo-catalytic degradation of methyl orange dye in aqueous media. *J. Environ. Chem. Eng.* **2018**, *6*, 218–227. [[CrossRef](#)]
20. Lutterbeck, C.A.; Wilde, M.L.; Baginska, E.; Leder, C.; Machado, Ê.L.; Kümmerer, K. Degradation of cyclophosphamide and 5-fluorouracil by UV and simulated sunlight treatments: Assessment of the enhancement of the biodegradability and toxicity. *Environ. Pollut.* **2016**, *208 Pt B*, 467–476. [[CrossRef](#)]
21. Kwon, M.; Kim, S.; Yoon, Y.; Jung, Y.; Hwang, T.M.; Lee, J.; Kang, J.W. Comparative evaluation of ibuprofen removal by $\text{UV}/\text{H}_2\text{O}_2$ and $\text{UV}/\text{S}_2\text{O}_8^{2-}$ processes for wastewater treatment. *Chem. Eng. J.* **2015**, *269*, 379–390. [[CrossRef](#)]
22. Zuorro, A.; Fidaleo, M.; Fidaleo, M.; Lavecchia, R. Degradation and antibiotic activity reduction of chloramphenicol in aqueous solution by $\text{UV}/\text{H}_2\text{O}_2$ process. *J. Environ. Manag.* **2014**, *133*, 302–308. [[CrossRef](#)] [[PubMed](#)]
23. Qiu, W.; Zheng, M.; Sun, J.; Tian, Y.; Fang, M.; Zheng, Y.; Zhang, T.; Zheng, C. Photolysis of enrofloxacin, pefloxacin and sulfaquinoxaline in aqueous solution by $\text{UV}/\text{H}_2\text{O}_2$, $\text{UV}/\text{Fe(II)}$, and $\text{UV}/\text{H}_2\text{O}_2/\text{Fe(II)}$ and the toxicity of the final reaction solutions on zebrafish embryos. *Sci. Total Environ.* **2019**, *651*, 1457–1468. [[CrossRef](#)] [[PubMed](#)]
24. Sánchez-Polo, M.; Daiem, M.M.A.; Ocampo-Pérez, R.; Rivera-Utrilla, J.; Mota, A.J. Comparative study of the photodegradation of bisphenol A by $\text{HO}\cdot$, SO_4^- and $\text{CO}_3^-/\text{HCO}_3^-$ radicals in aqueous phase. *Sci. Total Environ.* **2013**, *463–464*, 423–431.
25. Zhang, Y.; Xiao, Y.; Zhong, Y.; Lim, T. Comparison of amoxicillin photodegradation in the $\text{UV}/\text{H}_2\text{O}_2$ and $\text{UV}/\text{persulfate}$ systems: Reaction kinetics, degradation pathways, and antibacterial activity. *Chem. Eng. J.* **2019**, *372*, 420–428. [[CrossRef](#)]
26. Yin, K.; Deng, L.; Luo, J.; Crittenden, J.; Liu, C.; Wei, Y.; Wang, L. Destruction of phenicol antibiotics using the $\text{UV}/\text{H}_2\text{O}_2$ process: Kinetics, byproducts, toxicity evaluation and trichloromethane formation potential. *Chem. Eng. J.* **2018**, *351*, 867–877. [[CrossRef](#)]
27. Moon, B.R.; Kim, T.K.; Kim, M.K.; Choi, J.; Zoh, K.D. Degradation mechanisms of Microcystin-LR during UV-B photolysis and $\text{UV}/\text{H}_2\text{O}_2$ processes: Byproducts and pathways. *Chemosphere* **2017**, *185*, 1039. [[CrossRef](#)]
28. Oh, B.T.; Seo, Y.S.; Sudhakar, D.; Choe, J.H.; Lee, S.M.; Park, Y.J.; Cho, M. Oxidative degradation of endotoxin by advanced oxidation process ($\text{O}_3/\text{H}_2\text{O}_2$ & $\text{UV}/\text{H}_2\text{O}_2$). *J. Hazard. Mater.* **2014**, *279*, 105–110.
29. Lutze, H.V.; Bircher, S.; Rapp, I.; Kerlin, N.; Bakkour, R.; Geisler, M.; von Sonntag, C.; Schmidt, T.C. Degradation of chlorotriazine pesticides by sulfate radicals and the influence of organic matter. *Environ. Sci. Technol.* **2015**, *49*, 1673–1680. [[CrossRef](#)]

Publisher’s Note: MDPI stays neutral with regard to jurisdictional claims in published maps and institutional affiliations.



© 2020 by the authors. Licensee MDPI, Basel, Switzerland. This article is an open access article distributed under the terms and conditions of the Creative Commons Attribution (CC BY) license (<http://creativecommons.org/licenses/by/4.0/>).